

# EFFECTS OF ROTOR CONTAMINATION ON GYROPLANE FLIGHT PERFORMANCE

Holger Duda, Falk Sachs, Jörg Seewald, Claas-Hinrik Rohardt  
DLR (German Aerospace Center)  
Lilienthalplatz 7, 38108 Braunschweig, Germany

## Abstract

This paper describes the effects of rotor contamination on gyroplane flight performance such as its influence on propeller thrust required for cruise flight and takeoff distance. It is known from flight practice that rotor contamination due to insects degrades the flight performance of gyroplanes significantly. By flight trials with an MTOsport gyroplane this degradation has been quantified: in order to maintain altitude at 60 kt airspeed the engine rotational speed has to be increased by about 200 rpm due to the rotor contamination. Considering these experimental data in the simulation model shows that this means a performance degradation of about 14 %. In order to understand this significant effect an analysis has been conducted connecting these flight test results with the degradation of the airfoil performance due to contamination. The NACA 8-H-12 airfoil characteristics have been determined using XFOIL for the clean and the contaminated case. The drag coefficient computed with a fixed transition point near the leading edge (contaminated case) is almost doubled in the relevant region of lift coefficients compared to the free transition point calculation (clean case). Utilizing these aerodynamic characteristics within the overall MTOsport flight simulation model affirms the degradation measured in flight. Hence the computational results are considered to be valid and the simulation model can be applied to investigate potential flight performance improvements of future gyroplanes. Finally a simulation study of the takeoff performance with clean and contaminated rotor is presented indicating that the takeoff distance also increases by more than 16 %.

## 1. INTRODUCTION

A gyroplane is an aircraft that gets lift from a freely turning rotor and which derives its thrust from an engine-driven propeller [1]. Historically, this type of aircraft has been known as autogiro or gyrocopter. It was developed by Juan de la Cierva and in 1923 it was the first rotary-wing aircraft flying. Early gyroplanes were powered by engines in a tractor (pulling) configuration, like the Cierva C.30 from 1933 which was produced 180 times by 1945 [2].

Gyroplanes became largely neglected after significant improvements in helicopters. In the nineteen-fifties there was some revival of interest in the gyroplane by Igor Bensen's home-built gyroplane kits with an open airframe and the Fairey Company in Great Britain. Today in Europe several manufacturers sell single- and two-seater gyroplanes for the private aviation market. This boom can be explained by the fascinating flying characteristics in combination with the robustness and cost efficiency of this kind of air vehicle.

Figure 1 shows DLR's gyroplanes operated in Braunschweig for flight research.

The MTOsport (D-MTOS) has been used in flight test programs (2010 and 2012) for the validation of

simulation models and in addition to generate flight data to study gyroplane flight dynamics.

The Cavalon (D-MGTD) has a significant role in flight experiments in cooperation with the THW (German Federal Agency for Technical Relief). The aim of the project is to address how the gyroplane can be routinely operated for aerial reconnaissance use. The side-by-side configuration qualifies this type of gyroplane for demonstration flights.



MTOsport (D-MTOS)

Cavalon (D-MGTD)

**Figure 1: DLR's gyroplanes**

The ability of a gyroplane to fly very slowly, such as minimum airspeed of 20 kts, makes it very versatile and leads to extremely short takeoff and landing distances. The possibility to (almost) stop in the air and to descend vertically is a useful ability for observation flights. Compared to a fixed-wing airplane the gyroplane is relatively robust with respect to atmospheric disturbances and can be

operated safely under very gusty conditions. In case of an engine failure the rotor state does not change since it is in autorotation continuously.

The simplicity and the fascinating flying characteristics in combination with the robustness and cost efficiency of this kind of air vehicle explain the recent boom. This has been triggering DLR to put focus on modern gyroplanes [3-6]. DLR's main areas of interest contain the potential improvement of flight performance and comfort by advanced rotor systems utilizing more than two blades and advanced airfoils. Additionally the reduction of parasitic drag for higher cruise speeds by utilizing advanced rotor head designs and minimized fuselage drag are subjects of investigation. The research results are valuable for manufacturers with respect to overall system design and the development of larger gyroplanes with significantly higher performance and endurance. These advanced gyroplanes may take over several flying tasks in the future.

The objective of this paper is to investigate the influence of rotor blade contamination on the flight performance of a gyroplane. This investigation contributes to further understand potential improvements for future gyroplane developments.

## 2. GYROPLANE TECHNOLOGY

The gyroplane's appearance is quite similar to a helicopter. This is mainly due to the rotor system generating the lift force needed for flight. On the other hand it has components of an airplane like the landing gear, the tailplanes including a rudder as well as an engine providing forward thrust by a propeller. Its operation is similar to an airplane with a (short) takeoff run and a landing approach with a flare maneuver before touchdown.

### 2.1. Rotor System

The rotor system of today's lightweight gyroplanes is of significantly lower complexity than that of a helicopter, since no transmissions, gearboxes, tail rotors or driveshafts are needed. A teeter head rotor system is used which is commonly known as seesaw rotor, Figure 2. By control stick movements the rotor head can be tilted around the pitch pivot bolt (PPB) in order to tilt the rotor lift force forwards and backwards. Furthermore it can be moved around the roll pivot bolt (RPB) to control the attitude of the rotor lift force for rolling maneuvers.

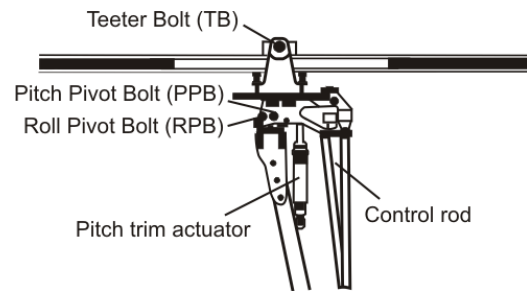


**Figure 2: Gyroplane tilting rotor system (AutoGyro's MTOsport)**

A tower block provides the attachment of the rotor to the rotor head by a central flapping hinge called teeter bolt (TB). This flapping hinge provides the freedom for the entire rotor to flap around the TB in order to compensate for asymmetric airflow and the resulting asymmetric lift distribution.

A pneumatic trim system provides additional control forces in order to improve flight comfort. A prerotation system allows an acceleration of the rotor to a speed of about 200 rpm before initiating the takeoff run.

The rotor blade airfoil utilized in several gyroplanes is the NACA 8-H-12 which is discussed in this paper. The rotor blades are connected to the rotor head with a fixed incidence angle. No collective blade control is available.

### 2.2. Airframe

The gyroplane airframe consists of the fuselage, the tailplanes, the engine and propeller, the landing gear and the control system. Gyroplanes with open and closed fuselages are available on the market.

The horizontal tailplane without elevator is needed for increased pitch damping in order to improve flight stability. The yawing movement of the gyroplane is controlled by a rudder like in an airplane. This is used to maintain coordinated flight by compensating yawing moments due to propeller slipstream effects and to perform crosswind landings.

The engine and propeller of today's gyroplanes are typically installed as pusher configurations. This allows an almost free vision in forward direction. The throttle is conventional to most powerplants and provides the means to increase or decrease engine power and thus, propeller thrust.

The landing gear contains two main wheels and a nose wheel, which is steerable and connected to the pedals. The main wheels contain the brakes.

The rotor control system consists of rods or cables transmitting the control stick movements to the rotor head.

### 2.3. Technical Data

Some basic data of DLR's gyroplanes are presented in Table 1.

	Cavalon D-MGTD	MTOsport D-MTOS
MTOW [kg]	500	450
Engine power [hp]	115	100
Rotor diameter [m]	8.4	8.4
Blade chord [m]	0.2	0.2
Blade incidence angle [°]	2.5	2.5
Cruise speed [kt]	60	60

Table 1: Technical data of DLR's gyroplanes

## 3. GYROPLANE FLIGHT PHYSICS

The following sections explain the basics of autorotation during vertical descent and forward flight as well as the drag force in cruise flight.

### 3.1. Vertical Autorotation

Autorotation is the self-sustained rotation of the rotor without the application of any shaft torque. The energy to drive the rotor is provided by the relative airstream.

During a vertical autorotation, two basic components contribute to the relative wind striking the rotor blades [1]. The upward flow through the rotor system remains relatively constant over the radial direction. It depends on the vertical descent rate of the rotor and the rotor-induced velocity.

The horizontal velocity component at the midpoint of a local blade section is depending on the rotor rotational speed and the radial position of the section. It is zero at the rotor shaft and reaches its maximum at the blade tip. The local lift and drag forces are depending on the local flow velocity and the angle of attack (AoA). During vertical descent the local AoA is decreasing in radial direction. This generates regions of the rotor disc that create the forces necessary for autorotation. The inner region, characterized by higher local AoA, creates driving aerodynamic force components due to forward tilted vectors of the resulting aerodynamic force, Figure 3. The outer region creates driven aerodynamic force components leading to an equilibrium state.

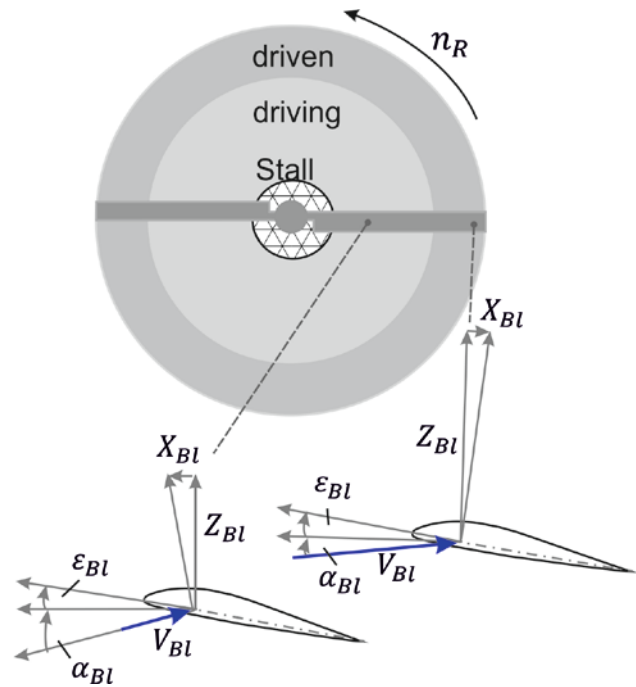


Figure 3: Regions of driving and driven aerodynamic forces (vertical autorotation)

The outer region with relatively smaller local AoA but higher velocities generates an aerodynamic force with a larger vertical component producing the majority of the rotor lift.

### 3.2. Autorotation in Forward Flight

In forward flight, an additional component of the airspeed contributes to the relative wind striking the rotor blades.

To prevent imbalanced lifting forces the rotor head is constructed such that the blades can flap. One or more teeter joint(s) is/are utilized for this purpose.

The advancing blade flaps up, decreasing the AoA, while the retreating blade flaps down, increasing the AoA. This leads to the effect that almost the entire retreating region is driving and the advancing region is driven during cruise flight, Figure 4.

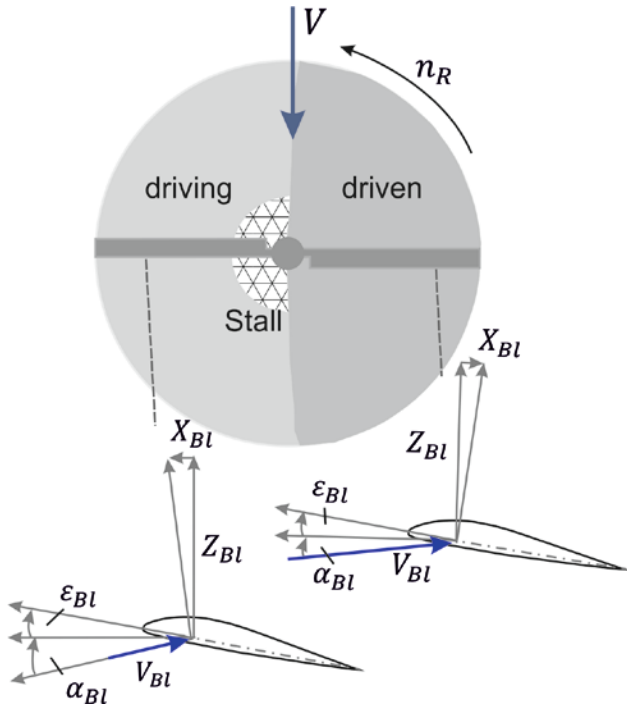


Figure 4: Regions of driving and driven aerodynamic forces (cruise flight)

### 3.3. Drag Force in Cruise Flight

The forces acting on the gyroplane during steady state horizontal cruise flight are presented in Figure 5. At an airspeed  $V = 60$  kt the longitudinal axis of the gyroplane may be considered to be almost parallel to the ground.

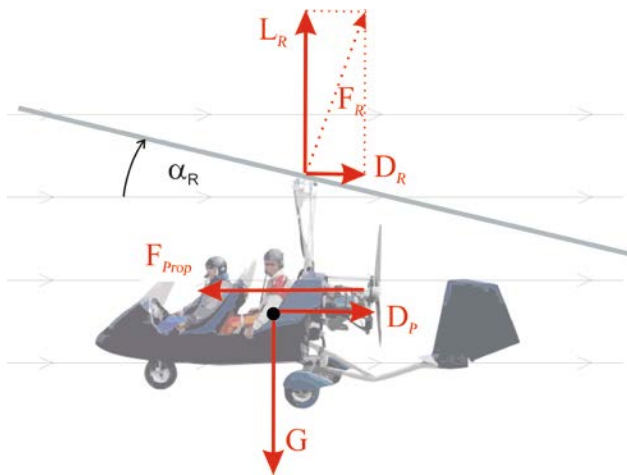


Figure 5: Forces acting on the gyroplane during steady state horizontal cruise flight (horizontal tail lift force neglected)

In this flight condition the lift force of the horizontal tail may be neglected; hence five important forces are considered to act on the gyroplane:

- $G$  Weight force acting in the center of gravity (CG) vertically downwards.
- $F_R$  Rotor force acting in the teeter bolt (TB) vertically to the rotor plane upwards.
- $D_P$  Parasitic drag force acting in the center of gravity parallel to the airflow backwards. It contains the drag from everything but the rotor blades, such as the fuselage, the gear, the tail, the rotor mast, the fittings, the rotor head, etc.
- $F_{Prop}$  Propeller force acting in the propeller shaft parallel to the longitudinal axis forwards.

The rotor force  $F_R$  is separated into lift and drag forces:

- $L_R$  Rotor lift force: part of the rotor force acting vertically to the airflow upwards.
- $D_R$  Rotor drag force: part of the rotor force acting parallel to the airflow backwards.

The total gyroplane drag force is due to the rotor and the parasitic part:

$$(1) \quad D = D_P + D_R.$$

The parasitic drag force is:

$$(2) \quad D_P = \frac{\rho}{2} \cdot V^2 \cdot S_P \cdot C_{DP}.$$

The rotor drag force arises by the tilting of the rotor force backwards due to the rotor AoA. Assuming that the rotor force acts approximately perpendicular to the rotor plane [10] the rotor drag force is:

$$(3) \quad D_R = F_R \cdot \sin \alpha_R \approx F_R \cdot \alpha_R.$$

Neglecting the relatively small vertical force acting on the horizontal tail and the small rotor AoA during steady state cruise flight, the rotor force can be assumed to be almost equal to the weight force:

$$(4) \quad F_R \approx G.$$

With this the total gyroplane drag force is:

$$(5) \quad D \approx \frac{\rho}{2} \cdot V^2 \cdot S_P \cdot C_{DP} + G \cdot \alpha_R.$$

For steady state flight the propeller force must be equal to the total drag force:

$$(6) \quad F_{Prop} = D \approx \underbrace{\frac{\rho}{2} \cdot V^2 \cdot S_P \cdot C_{DP}}_{D_P} + \underbrace{G \cdot \alpha_R}_{D_R}.$$

It is obvious that during low-speed flight the rotor drag force is dominant due to the high rotor AoA at this flight state. At higher airspeeds the parasitic drag force becomes more relevant for the overall drag force.

#### 4. GYROPLANE SIMULATION MODEL

An overall simulation model of the MTOsport gyroplane is available at DLR. The simulation model is implemented in MATLAB/Simulink<sup>®</sup> and contains subsystems for the rotor, the body, the landing gear, the control system, the engine and the propeller.

The rotor is calculated by the strip method, such that the individual airflows and aerodynamic forces at ten blade elements are computed. The rotor blades are considered to be rigid. The rotor-induced velocity is a function of rotor force, rotor disk area and airspeed and -direction. The rotor rotational speed is determined by a first-order differential equation based on the rotational moment of both blades. The flapping motion of the rotor blades is considered as well as generic aerodynamic effects due to Mach number and tip loss.

The total aerodynamic forces and moments of the gyroplane body including mast and tailplanes are determined. A landing gear model is available as well as a model of the control system providing the stick force/deflection relation. An engine model of the Rotax 912 is available providing propeller thrust depending on propeller rotational speed and airspeed beneath others.

The simulation model of the MTOsport has been validated with flight test data. For this purpose the MTOsport (D-MTOS) has been equipped with a special flight test instrumentation (FTI), Figure 6.



Figure 6: *MTOsport gyroplane with special flight test instrumentation during flight test*

The measured flight parameters were sufficient to fully understand the entire flight state of the gyroplane body and rotor.

Inertial data, control deflections and forces, airflow data as well as rotor and propeller rotational speed were recorded. In order to deliver high quality measurements of the airflow a nose boom with a length of more than two meters has been installed. At its tip special vanes for measuring angle of attack and sideslip have been installed.

The flight test data were utilized to validate the simulation model of the MTOsport. The simulation model matches the flight test data adequately for several maneuvers like steady state flights in the entire airspeed range, dynamic maneuvers in the roll, pitch and yaw axes as well as acceleration and deceleration flights [3].

The simulation model is part of the gyroplane flight simulator operated at DLR, Figure 7.



Figure 7: *DLR's gyroplane flight simulator*

This flight simulator is used for pilot training and handling qualities studies of new developments.

## 5. EFFECTS OF ROTOR CONTAMINATION

### 5.1. Flight Trials

In order to quantify the effects of rotor contamination flight trials with the MTOsport gyroplane were conducted. The gyroplane was flown with contaminated and clean rotor blades within one hour. No atmospheric differences between the two flights were noticeable.

Figure 8 shows the level of rotor blade contamination by insects. This is a typical look of the rotor blades after flight in the summer period. It may look like this or even worse after less than one hour of flight time.

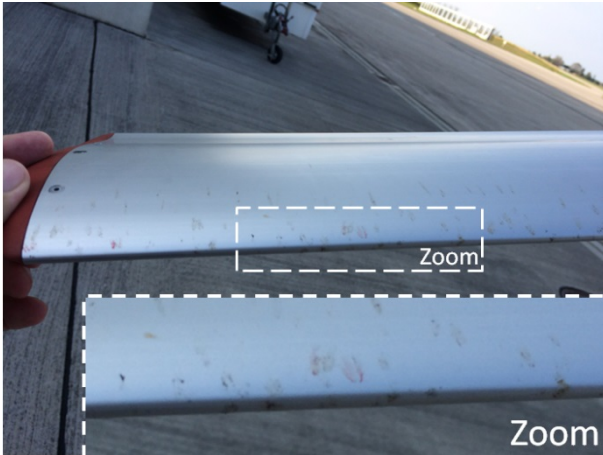


**Figure 8: Gyroplane rotor blade contaminated by insects**

In both flights the gyroplane has been trimmed at an airspeed of  $V \approx 60$  kt while the engine and rotor rotational speeds have been measured. The basic results obtained from these two flights are summarized in Table 2:

Rotor	$V$ [kt]	$n_{Prop}$ [rpm]	$n_R$ [rpm]
Clean	$\approx 60$	$\approx 4400$	$\approx 350$
Contaminated	$\approx 60$	$\approx 4600$	$\approx 350$

**Table 2: Flight test results with clean and contaminated rotor**

In order to maintain altitude the engine rotational speed has to be increased by about

$$\Delta n_{Prop} \approx 200 \text{ rpm}$$

due to the rotor contamination. (Note: this is the engine rotational speed; the propeller rotational speed is lower by the factor 0.41 due to gearing).

The rotor rotational speed is not affected by the rotor blade contamination.

## 5.2. Analysis

For the analysis of the rotor contamination effects the MTOsport simulation model has been used combined with a 2D airfoil calculation.

### 5.2.1. Airfoil Aerodynamic Characteristics

The aerodynamic characteristics of the NACA 8-H-12 airfoil based on wind tunnel tests are published in [7]. However, the effects of contamination are not available.

For this purpose a calculation using XFOIL, Version 6.94 [8], has been conducted at different airspeeds for the two cases

1. "Clean": laminar-turbulent transition point free (means to be determined by XFOIL) and
2. "Contaminated": laminar-turbulent transition point fixed at 7 % of the blade chord.

The "fixed transition point" represents a turbulent boundary layer over nearly the entire surface due to the contamination. The transition from laminar to turbulent is forced at 7 % of the blade chord at the upper and the lower surface. This is quite far upstream in comparison to the "free transition point" calculation where the airflow is laminar up to about 50 % of chord on the upper surface and to 100 % of chord on the lower surface depending on Reynolds number and AoA. The fixation on 7 % of the blade chord is based on long term experience in the field of laminar-turbulent transition research [9].

Figure 9 presents the computational results for a Reynolds number of 1.9 million and a Mach number of 0.41. This case corresponds to a rotor blade local velocity of about  $V_{Bl} \approx 270$  kt and a blade chord of 0.2 m of the MTOsport rotor. This represents the average Reynolds number for cruise at about 90 % radial position and a typical rotor rotational speed of  $n_R \approx 350$  rpm.

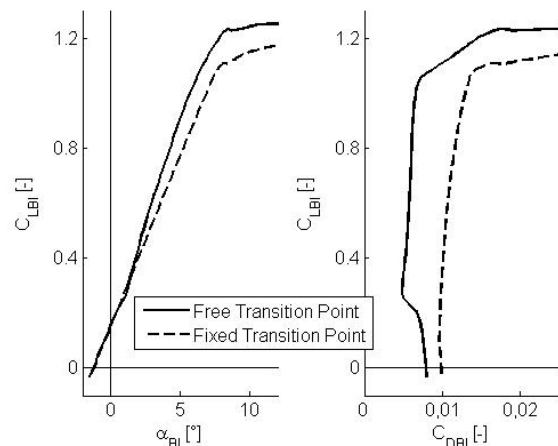


**Figure 9: Computed aerodynamic characteristics of the NACA 8-H-12 airfoil, 2D calculation (Reynolds number of 1.9 million, Mach number of 0.41)**

It appears that the drag coefficient  $C_{DBI}$  computed with a fixed transition point is almost doubled in the relevant region of local lift coefficients:

$$C_{LBI} \approx 0.3 \dots 1.0.$$

According to this calculation, the airfoil produces about 100 % more drag due to turbulent boundary layer caused by this contamination.

Furthermore, the lift curve slope with respect to rotor blade local AoA is reduced by about 15 % in the case of fixed transition, representing the contaminated case.

In case of stronger rotor blade contamination further degradation with respect to drag and maximum lift coefficients may occur.

### 5.2.2. Simulated Cruise Flight

The simulation model of the MTOsport gyroplane has been used to investigate the impact of rotor contamination on flight performance. Standard atmosphere and a total aircraft mass of  $m = 450$  kg were assumed. With these assumptions the simulation model has been trimmed at an airspeed of  $V = 60$  kt using the aerodynamic characteristics presented in Figure 9.

In both cases, i.e. "clean" and "contaminated," the rotor force is

$$F_R \approx G \approx 4414 \text{ N}.$$

It can be assumed that the parasitic drag force remains unchanged due to contamination. With the parasitic drag area of

$$S_p = 1.0 \text{ m}^2$$

and a parasitic drag coefficient of

$$C_{DP} = 1.0$$

a parasitic drag force of

$$D_p = 573 \text{ N}$$

is obtained at  $V = 60$  kt according to eq. (2).

Table 3 presents the trim results based on the simulation model for the clean and contaminated cases.

	Clean	Contaminated
$n_R$ [rpm]	347	348
$\alpha_R$ [°]	6.2	8.1
$n_{Prop}$ [rpm]	4401	4596
$D_R$ [N]	478	624
$D_p$ [N]	573	573
$F_{Prop}$ [N]	1051	1197
$L/D$ [1]	4.2	3.7

**Table 3: MTOsport simulation model trimmed at an airspeed of  $V = 60$  kt for clean and contaminated rotor**

The engine rotational speed is increased by

$$\Delta n_{Prop} = 195 \text{ rpm}$$

which fits the flight test results very well. The difference of propeller thrust needed for steady state flight is:

$$\Delta F_{Prop} = 1197 \text{ N} - 1051 \text{ N} = 146 \text{ N}.$$

This means a relative increase of about 14 % due to the contamination. It can be assumed that the fuel consumption would rise by the same amount.

Obviously, the rotor blade local AoA is also increased due to the contamination. At a given airspeed it depends on the blade azimuth angle and the radial position.

Figure 10 shows the rotor blade local AoA in cruise flight at a radial position of about 90 % of the rotor radius.

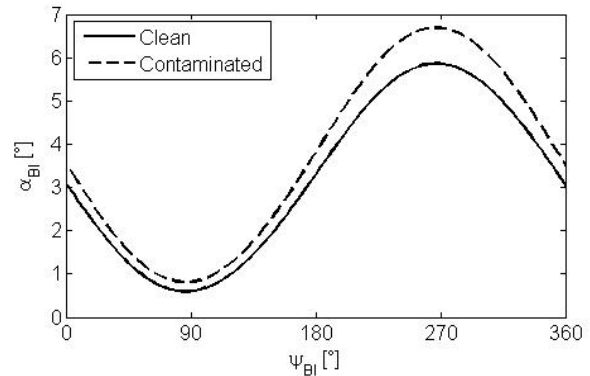


**Figure 10: Rotor blade local AoA at a radial position of about 90 % of rotor radius in cruise flight condition**

The blade azimuth angle is defined to be zero when the rotor blade is at the rear position.

For the clean case the maximum rotor blade local AoA is about  $\alpha_{BI} \approx 5.9^\circ$  for the retreating blade ( $\psi_{BI} = 270^\circ$ ). For the contaminated case  $\alpha_{BI} \approx 6.7^\circ$  is obtained. This confirms the need for higher rotor AoA for the contaminated case.

### 5.2.3. Simulated Takeoff

The takeoff procedure to be applied for a gyroplane with a tilting rotor system is as follows:

- (1) Prerotate up to a sufficient rotor rotational speed ( $n_R = 200$  rpm) while the control stick is in full forward position.
- (2) Release the wheel brake.
- (3) Move the control stick to full aft position.
- (4) Apply full throttle.

- (5) Accelerate on ground.
- (6) Control pitch angle via control stick during takeoff.
- (7) Accelerate in flight up to about  $V = 50$  kt and climb.

The takeoff acceleration with the rotor disc tilted aft allows airflow through the blades to accelerate the rotor. After takeoff the pilot needs to push the control stick forward in order to lower the rotor AoA and control the pitch attitude.

For the MTOsport a prerotation up to  $n_R = 200$  rpm is needed in order to avoid the so called "blade flapping". This phenomenon is caused by too low rotor rotational speed at too high airspeed and can be catastrophic.

For the simulation of the complex takeoff procedure a simple pilot model has been used in order to obtain comparable results for the clean and contaminated cases.

In both cases (clean und contaminated) an initial rotor rotational speed of  $n_R = 200$  rpm is assumed.

The control stick in full aft position results in a rotor head pitch control angle of  $\eta_{RH} = 15^\circ$ .

Assuming the longitudinal axis of the gyroplane to be parallel to the ground, the rotor AoA during the takeoff acceleration on the runway is:

$$(8) \quad \alpha_R = \eta_{RH} + \beta_{\max} \cdot$$

During takeoff and once airborne the rotor head angle is lowered by the pilot model for pitch control. By this the rotor AoA is lowered as well.

The maximum takeoff thrust of the MTOsport engine (Rotax 912) is about  $F_{Prop} \approx 2000$  N.

Figure 11 presents the results of a simulated takeoff run of the MTOsport with clean rotor. Standard atmosphere and no wind were assumed.

The takeoff roll distance of the MTOsport with clean rotor is about  $s_{TO} \approx 121$  m according to this simulation. The distance to pass 15 m height above ground is  $s_{15} \approx 218$  m. These values correspond well with flight experience.

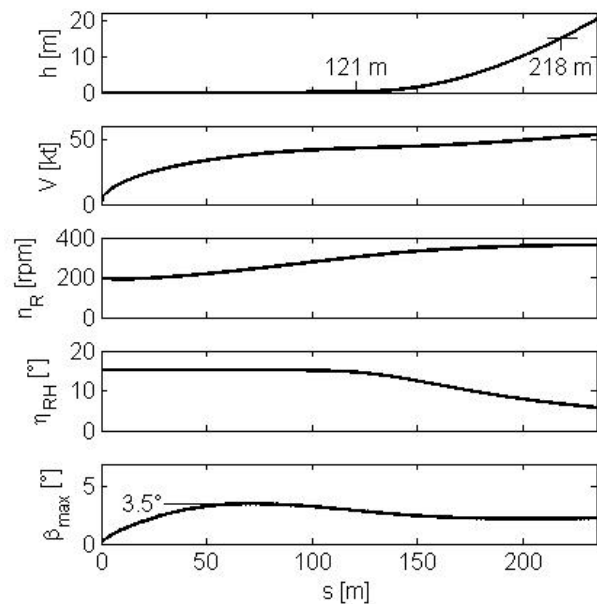


**Figure 11: Simulated takeoff run with clean rotor (mass 450 kg)**

The MTOsport is taking off at an airspeed of  $V = 43$  kt. At 15 m height the gyroplane has accelerated to  $V = 51$  kt. Its rotor rotational speed rises from  $n_R = 200$  rpm after prerotation to  $n_R \approx 300$  rpm at takeoff and  $n_R \approx 350$  rpm during steady state cruise flight.

The maximum flapping angle is obtained shortly before takeoff. Its value  $\beta_{\max} = 3,5^\circ$  is well below the flapping hinge stops of approximately  $7^\circ$ .

The takeoff simulation has also been conducted with the contaminated rotor. The results are presented in Table 4.

	Clean	Contaminated
$s_{TO}$ [m]	121	144
$s_{15}$ [m]	218	253
$\beta_{\max}$ [°]	3.5	4.2

**Table 4: Simulated MTOsport takeoff performance with clean and contaminated rotor**

The takeoff roll distance is increased by about 20 % due to rotor contamination. The distance to pass the 15 m height is increased by about 16 %.

Interesting to note is that the maximum flapping angle is increased by 20 % to  $\beta_{\max} = 4,2^\circ$ . Hence the margin to the flapping hinge stops is reduced.

## 6. DISCUSSION

The analysis highlights the significant effect of rotor contamination on gyroplane flight performance. The drag created by the NACA 8-H-12 airfoil is increased by about 100 % due to the contamination investigated herein. This immense aerodynamic degradation leads to an overall performance loss of the gyroplane by about 14 % with respect to cruise flight performance and up to 20 % longer takeoff distance.

It appears that gyroplane flight performance could be improved by even longer laminar airflow on the airfoil. However, rotor contamination cannot be avoided since insects are permanently populating the air. This makes the approach to achieve longer laminar airflow questionable.

For a comparison the helicopter airfoil NACA 23012 has been calculated using XFOIL with the input data presented in section 5.2.1. Table 5 presents the results for a local rotor blade lift coefficient of  $C_{LBI} = 0.8$ .

	Free	Fixed
NACA 8-H-12	$C_{DBI} = 0.006$	$C_{DBI} = 0.012$
NACA 23012	$C_{DBI} = 0.008$	$C_{DBI} = 0.012$

**Table 5: Rotor local drag coefficients calculated with XFOIL for fixed and free transition (Reynolds number 1.9 million, Mach number 0.41)**

The degradation due to contamination of the NACA 23012 airfoil is “only” 50 % instead of 100 % in case of the NACA 8-H-12. The aerodynamic quality of the NACA 8-H-12 clean airfoil is very high even though it is a quite old design.

There might be options to improve the gyroplane performance by airfoil optimization, but its robustness against contamination is an issue. Instead gyroplane manufacturers might obtain significant cruise flight performance benefits by

1. reducing the parasitic drag force and/or
2. adding a fixed wing.

In order to reduce the parasitic drag force a redesign of all obviously aerodynamic unfavorably shaped parts like the rotor head, the mast or the gear is needed.

Another approach is the unloading of the rotor by an additional fixed wing producing lift. An additional wing can minimize the overall drag drastically in the intermediate velocity range. Calculations for a representative gyroplane with an additional wing of just 1.7 m<sup>2</sup> area show a reduction of about 12 % total drag at cruise speed [6].

## 7. CONCLUSIONS

The analysis presented herein improved the understanding of gyroplane flight performance, particularly the influence of rotor airfoil aerodynamic quality on air vehicle flight performance.

Based on these results the following conclusions can be drawn

1. Rotor blade contamination by insects may lead to significant performance degradations. The propeller thrust in cruise flight is about 14 % higher. The takeoff distance raises more than 16 %.
2. DLR's gyroplane simulation model is capable to assess individual rotor aerodynamic effects on overall aircraft level.
3. The NACA 8-H-12 airfoil used in most of today's gyroplanes has a high aerodynamic quality if the surface is clean.
4. Further reduction of rotor blade airfoil drag by even longer laminar airflow might be nullified by contamination which in practice cannot be avoided.

## 8. SYMBOLS AND ABBREVIATIONS

Greek symbols

$\alpha_R$	Rotor angle of attack [°]
$\alpha_{BI}$	Rotor blade local angle of attack [°]
$\beta_{max}$	Maximum flapping angle [°]
$\varepsilon_{BI}$	Rotor blade incidence angle [°]
$\eta_{RH}$	Rotor head pitch control angle [°]
$\psi_{BI}$	Rotor blade azimuth angle [°]

Latin symbols

$C_{DBI}$	Rotor blade local drag coefficient [-]
$C_{LBI}$	Rotor blade local lift coefficient [-]
$C_{DP}$	Gyroplane parasitic drag coefficient [-]
$D$	Total gyroplane drag force [N]
$D_P$	Gyroplane parasitic drag force [N]
$D_R$	Rotor drag force [N]
$F_{Prop}$	Propeller force [N]
$F_R$	Rotor force vertical to rotor plane [N]
$G$	Weight force [N]
$L_R$	Rotor lift force [N]

$n_{Prop}$	Engine rotational speed [rpm]
$n_R$	Rotor rotational speed [rpm]
$r_R$	Rotor radius [m]
$S_P$	Parasitic drag area [m <sup>2</sup> ]
$S_{15}$	Distance to pass 15 m obstacle [m]
$S_{TO}$	Takeoff run distance [m]
$V$	Airspeed [kt]
$V_{Bl}$	Rotor blade local velocity [kt]
$X_{Bl}$	Rotor blade local horizontal force [N]
$Z_{Bl}$	Rotor blade local vertical force [N]

#### Abbreviations

AoA	Angle of Attack
CG	Center of Gravity
DLR	Deutsches Zentrum für Luft- und Raumfahrt (German Aerospace Center)
FTI	Flight Test Instrumentation
MTOW	Maximum Takeoff Weight
PPB	Pitch Pivot Bolt
RPB	Roll Pivot Bolt
TB	Teeter Bolt
THW	Technisches Hilfswerk (German Federal Agency for Technical Relief)

## 9. REFERENCES

- [1] Leishman, J. G., "Development of the Autogiro: A Technical Perspective", *Journal of Aircraft*, Vol. 41, No. 4, pp. 765-781, 2004.
- [2] Harris, F.D., "Introduction to Autogyros, Helicopters, and Other V/STOL Aircraft, Volume I: Overview and Autogyros", NASA/SP-2011-215959 Vol I, Moffett Field, 2011.
- [3] Pruter, I. and Duda, H., "A new Flight Training Device for Modern Lightweight Gyroplanes", American Institute of Aeronautics and Astronautics, AIAA – Modeling and Simulation Technologies Conference, Portland, 2011.
- [4] Duda, H., Pruter, I., Deiler, C., Oertel, H., Zach, A., "Gyroplane Longitudinal Flight Dynamics", 3rd CEAS Air & Space Conference, Venice, 2012.
- [5] Duda, H., Seewald, J., Cremer, M., "Data Gathering for Gyroplane Flight Dynamics and

Simulation Research", 24th SFTE-EC Symposium, Braunschweig, 2013.

[6] Sachs, F., Duda, H., Seewald, J., „Leistungssteigerung von Tragschraubern durch Starrflügel“, Deutscher Luft- und Raumfahrt-kongress, Augsburg, 2014.

[7] Schaefer, R. and Smith, H. A., "Aerodynamic Characteristics of the NACA 8-H-12 Airfoil", NACA TN 1998, Langley, 1949.

[8] Drela, M., "XFOIL: An Analysis and Design System for Low Reynolds Number Airfoils", MIT Dept. of Aeronautics and Astronautics, Cambridge, Massachusetts, USA, 1989.

[9] Harris, C., "Two-Dimensional Aerodynamic Characteristics of the NACA 0012 Airfoil in the Langley 8-Foot Transonic Pressure Tunnel", NASA TM 81927, Langley, 1981.

[10] Prouty, R. W., "Helicopter Aerodynamics - Ray Prouty's Rotor and Wing Columns 1979-1992", Helobooks, a unit of Mojave Books LLC, Mojave CA, 2004.